Amorphous In-Ga-Mg-O Thin Films Formed by RF Magnetron Sputtering: Optical, Electrical Properties and Thin-Film-Transistor Characteristics

HISATO YABUTA [1], **NAHO ITAGAKI** [1], **TOSHIKAZU EKINO**[2], **AND YUZO SHIGESATO**[3]

[1]Graduate School of Information Science and Electrical Engineering, Kyushu University, Fukuoka 819-0395, Japan
[2]Graduate School of Advanced Science and Engineering, Hiroshima University, Higashi-Hiroshima 739-8521, Japan
[3]Graduate School of Science and Engineering, Aoyama Gakuin University, Sagamihara 252-5258, Japan

CORRESPONDING AUTHOR: HISATO YABUTA (e-mail: yabuta.hisato.475@m.kyushu-u.ac.jp)

ABSTRACT We report on optical and electrical properties of amorphous In-Ga-Mg-O (a-IGMO) films and characteristics of a-IGMO channel thin-film transistors which went through the reductive post-annealing process. Optical band-gap energies of a-IGMO films were larger than that of amorphous In-Ga-Zn-O (a-IGZO) films. Carrier density and Hall mobility of a-IGMO films with the reductive post-annealing were almost the same degree as those of a-IGZO films. Although the reductive annealing with the SiN_x underlayer makes an a-IGZO film degenerate semiconductor and its TFT inoperative, a-IGMO TFTs successfully operated after this reductive process. Break-junction tunnelling spectroscopy which was applicable not to a-IGMO but to a-IGZO with the reductive process showed a noticeable density of state character in the vicinity of the Fermi level for a-IGZO, which is consistent with its property.

INDEX TERMS Amorphous materials, semiconductor-insulator interfaces, semiconductor materials, semiconductor materials measurements, thin film transistors, tunneling.

I. INTRODUCTION

Amorphous In-Ga-Zn-O (a-IGZO) films have attracted much attention because a-IGZO channel thin-film-transistors (TFTs) can be fabricated at low temperatures, which show remarkable electrical performances, such as high field-effect mobility of $\mu_{FE} \sim 10$ cm^{2}V^{-1}s^{-1} [1] compared to the conventional hydrogenated amorphous silicon (a-Si:H) TFTs, and are compatible with large-area fabrication and mass production using conventional rf magnetron sputtering deposition [2]. These sputtering-formed a-IGZO channel TFTs have intensively been developed to apply to active matrix (AM) flat panel displays (FPDs), especially large-scale or/and high-performance liquid crystal displays (LCDs) and organic light-emitting diode (OLED) displays. Nowadays, a-IGZO TFTs have been employed in many types of commercial AM-FPDs, e.g., high resolution AM-LCDs and AM-OLED displays in smartphones and tablet PCs [3].

On the other hand, a-IGZO TFT and similar oxide-semiconductor TFTs have been investigated to fabricate in the back end of line (BEOL) for 3-dimensional (3D) integrated circuits (ICs) with silicon complementary metal-oxide-semiconductor (CMOS) elements because of their low temperature fabrication process (<400 °C) and high field-effect mobility. However, annealing process in hydrogen-containing atmosphere which has been employed in BEOL process for terminating defects in silicon generates extra carriers in the a-IGZO channel layer, resulting in degradation of the BEOL-TFTs in 3D CMOS ICs. A possible approach to solve this problem should be employ a channel material endurable against reductive process, same as the amorphous In-Ga-Si-O [4].

As a channel material for BEOL-TFTs, we have focused on In-Ga-Mg-O system, which has similar crystalline phase to the In-Ga-Zn-O system, and shows the wider bandgap
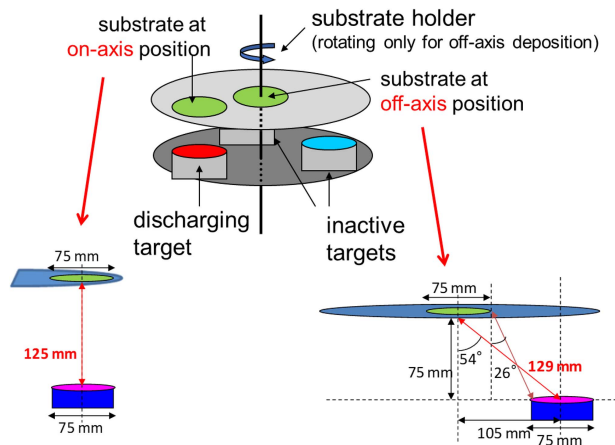
FIGURE 1. Schematic illustration of target-substrate geometries in the rf magnetron sputtering apparatus which we employed in this study: On-axis geometry (face-to-face) without substrate-holder rotation, and off-axis geometry (diagonal) with substrate-holder rotation.

energy and the lower carrier density with only slightly larger carrier effective mass than those of the In-Ga-Zn-O [5], [6], [7]. Therefore, we expected that amorphous In-Ga-Mg-O (a-IGMO) films and a-IGMO TFTs show similar electrical property and TFT characteristics when extra carrier generates in the films by the reductive process. In this study, we examined optical, electrical properties and TFT characteristics of a-IGMO films and TFTs formed by rf magnetron sputtering with a reductive post-annealing process.

II. EXPERIMENTAL DETAILS

Amorphous IGMO films were deposited by rf magnetron sputtering using 3-inch-diameter polycrystalline $InGaMgO_4$ or $In_2Ga_2MgO_7$ ceramic target (both supplied by Toshima Manufacturing Co., Ltd.) with two types of target-substrate geometries: an on-axis (face-to-face) geometry without substrate-rotation and an off-axis (diagonal) geometry with location of substrate diagonally opposite of a target at an angle of ∼35° to the target surface with distance between target-center and substrate-center of 130 mm with substrate-rotation at about 10 revolutions per minutes (see Fig. 1). Since a face-to-face geometry is usually employed in the industrial practical process of sputtering deposition, the on-axis deposition was favorable in this study, taking a practical application of a-IGMO films into account. However, a direct plasma irradiation to the film at the on-axis geometry sometimes affects the depositing film harmfully, especially for keeping the films amorphous. Therefore, we examined the films deposited not only at the on-axis geometry but also at the off-axis one.

For the deposition, we employed an input rf power of 200 W, a sputtering gas of 1%-O_2/99%-Ar under a pressure of 0.50 Pa, and no intentional substrate heating. For the fabrication of bottom-gate-type TFTs, 200 nm-thick SiN_x gate insulators were deposited by plasma-enhanced chemical-vapor-deposition (PECVD) with substrate temperature of 340 °C over defined Mo (50 nm) gate electrodes on glass

substrates (Corning #1737). After deposition of a-IGMO films on the SiN_x insulators, the samples were annealed at 300 °C in N_2; this post-annealing process is reductive one because hydrogen in the SiN_x layer diffuses into a-IGMO by annealing as mentioned below. Subsequently, Au (100 nm)/Ti (5 nm) films for source/drain electrodes were deposited by electron-beam (EB) evaporation. Photolithography, dry etching (for Mo, SiN_x) and lift-off (for a-IGMO, Au/Ti) techniques were employed for patterning these components of the TFTs.

Characteristics of the a-IGMO TFTs were measured with a semiconductor characterization system (Keithley 4200). Field-effect mobility, μ_{FE}, and threshold voltage, V_t, were derived from the relation $I_D = (\mu_{FE}C/2)\cdot(W/L)\cdot(V_G - V_t)^2$ (I_D: source-drain current, C: capacitance of the gate insulator, W/L: ratio of width to length of the channel, V_G: gate voltage) in the saturation region of $V_D > V_G - V_t$ (V_D: source-drain voltage).

A parallel beam x-ray diffractometer (Philips X'pert MRD) with a multilayer x-ray mirror was employed for x-ray diffraction (XRD) measurements using Cu-Kα x-ray beam. Optical transmission and reflection spectra were taken at wavelength range of 240–2400 nm using Hitachi U-4100 spectrometer to estimate optical absorption coefficient α. Electrical conductivity and Hall coefficient measurements were carried out at room temperature by van der Pauw method using a Hall effect measurement system (Accent HL5500PC) with a high-resistivity buffer amplifier. Au (100 nm)/Ti (5 nm) electrode pads for the Hall samples were deposited by EB evaporation with shadow-masks, and voltage among electrodes of ∼20 mV and magnetic field of 0.5 Tesla were applied at the Hall measurement. In order to obtain information about the bandgap and the in-gap states of these amorphous oxide semiconductors, break-junction tunnelling spectroscopy (BJTS) [8], [9] was attempted. A rectangular strip-shaped small piece of conductive film sample on insulating substrate whose both ends were electrically wired and mechanically fixed was clacked under liquid helium by applying adjustable bending force on the back surface. This technique realizes a very clean tunnel-junction interface with an insulating gap of more or less than 1 nm in width. The tunnel spectrum, i.e., the differential conductivity dI/dV, where I and V are the tunnel current and the bias voltage, respectively, is superposition of spectra from a myriad of local junctions generated at the crack, unlike a spectrum from one rigid junction (tip/gap/sample-surface) in scanning tunnel spectroscopy. However, a tunnel spectrum of BJTS certainly involves essential information of the sample owing to its clean and fresh junction created each time.

III. RESULTS AND DISCUSSION

Fig. 2 shows XRD charts of IGMO films (about 200 nm in thickness) deposited using $InGaMgO_4$ and $In_2Ga_2MgO_7$ (abbreviated to IGMO111 and IGMO221, respectively) ceramic targets at off-axis (diagonal) and on-axis (face-to-face) geometries. The deposition durations for IGMO films (200 nm in thickness) at off-axis and on-axis geometries were about 30 and 10 minutes, respectively, and it had been confirmed that
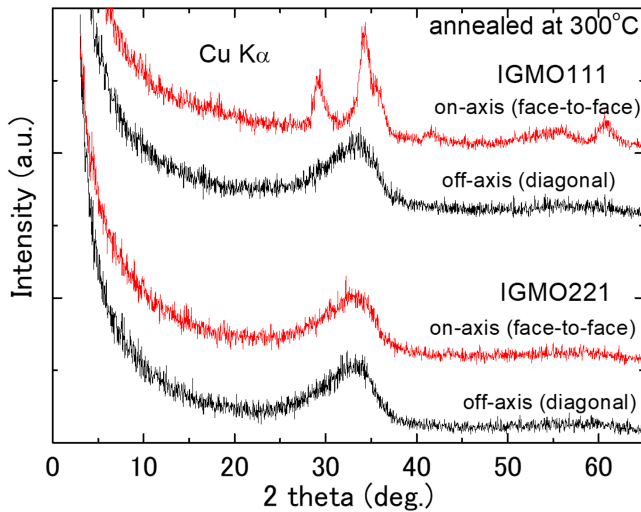
FIGURE 2. X-ray diffraction patterns taken by the 2θ-ω method of IGMO111 and IGMO221 films (about 200 nm in thickness) both deposited with on-axis (face-to-face) and off-axis (diagonal) geometries.

FIGURE 3. Photon energy $h\nu$ dependence of optical absorption coefficient α plotted as $(\alpha h\nu)^{1/2}$ vs $h\nu$ for as-deposited and annealed (300 °C in N$_2$) films of (a) a-IGMO111 and (b) a-IGMO221. Optical bandgap energy E_{go} estimated from the x-intercept of linear relation of $(\alpha h\nu)^{1/2}$ vs $h\nu$ for each sample was indicated in the figure. Decrease of $(\alpha h\nu)^{1/2}$ with increasing $h\nu$ at high photon energies ($h\nu > \sim 4.5$ eV) is due to optical absorption by PECVD-SiN$_x$, because the films on silica substrates show almost the same behavior of $(\alpha h\nu)^{1/2}$ at $h\nu < \sim 4.5$ eV and no decrease at $h\nu > \sim 4.5$ eV.

the surface temperature of the films rose to about 150 °C or less after the sputtering deposition. These films were amorphous even after annealing at 300 °C, except the IGMO111 film deposited at on-axis geometry. The diffraction peaks for the IGMO111 film with on-axis deposition can be identified as spinel-type In$_2$MgO$_4$ and rock salt-type MgO crystals. This means that IGMO111 is rather instable and easily decomposed to the secondary phases by direct (facing) exposure of sputtering plasma, compared to IGMO221. Hereafter, we employed only the off-axis geometry for preparing amorphous (a-) IGMO111 films.

Dependences of optical absorption coefficient α on photon energy $h\nu$ for as-deposited and annealed (300 °C in N$_2$) films of a-IGMO111 and a-IGMO221 are shown in Fig. 3(a) and (b), respectively. The optical absorption of each film well obeys the relation of $(\alpha h\nu)^{1/2}$ vs $h\nu$ [10], which is usually employed to estimate optical bandgap energy E_{go} of amorphous substances. E_{go} values of a-IGMO111 and a-IGM221 films are about 3.4 and 3.2–3.3 eV, respectively, which are slightly larger than that of a-IGZO films deposited with almost the same conditions ($\sim$3.1 eV) [11] and smaller than that of polycrystalline InGaMgO$_4$ ceramics ($\sim$4.2 eV) [6]. The curves of $(\alpha h\nu)^{1/2}$ are slightly shifted to the higher photon energies by annealing as the shift of a-IGZO films; these shifts should be caused not by the Burstein-Moss effect but perhaps by a structural relaxation because of no-degeneracy [11].

Hall effect measurement revealed that carrier density and Hall mobility of post-annealed (300 °C in N$_2$) a-IGMO221 film (deposited at on-axis geometry) on SiN$_x$ are 5×10^{17} cm^{-3} and 7 cm^{2}V^{-1}s^{-1}, respectively. Since these values are similar to those of annealed a-IGZO films on glass [11], a-IGMO films on SiN$_x$ perhaps show good electrical performance as a channel semiconductor material like a-IGZO. In the case of a-IGMO111 film (deposited at off-axis geometry)
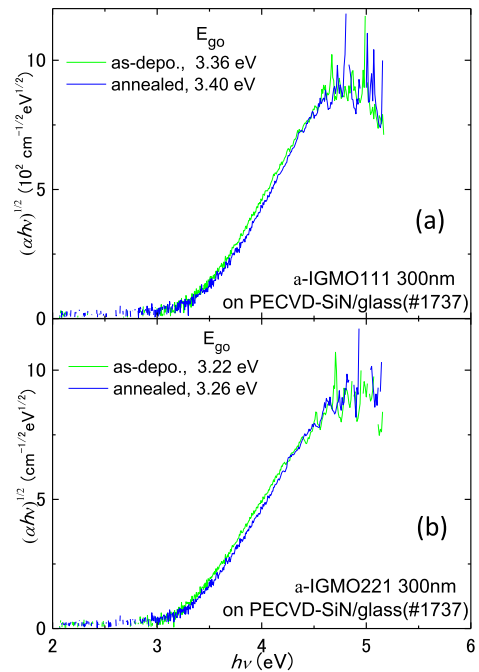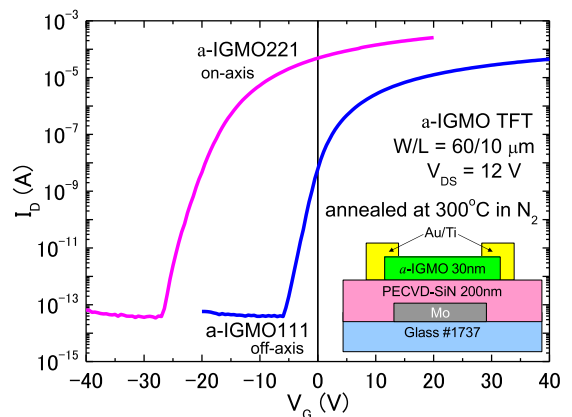

FIGURE 4. Transfer characteristics of a-IGMO111 and a-IGMO221 TFTs. Schematic drawing in the figure illustrates the structure of measured a-IGMO TFTs.

on SiN$_x$, resistivity was too high to measure Hall coefficient even after the post-annealing.

TFT characteristics of a-IGMO TFTs with a-IGMO111 and a-IGMO221 channels are shown in Fig. 4, and structure of the a-IGMO TFT is shown in the inset. These a-IGMO TFTs show good operations; the estimated μ_{FE} and V_t are 0.42 cm^{2}V^{-1}s^{-1} and +1.4 V (enhancement mode operation) for a-IGMO111 TFT, and 2.6 cm^{2}V^{-1}s^{-1} and -15 V (depletion mode operation) for a-IGMO221 TFT, respectively. In the
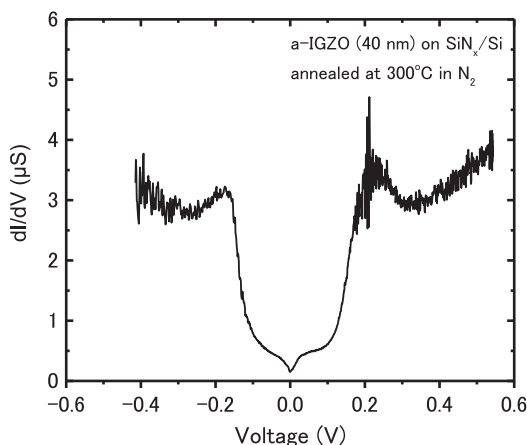
FIGURE 5. A tunnelling spectrum (tunnelling conductance *dI/dV* vs bias voltage) of a conductive a-IGZO film on SiN$_x$/Si with post-annealing process at 300 °C in N$_2$.

case of a-IGZO films deposited with the same condition as these a-IGMO films, TFT with a-IGZO channel on PECVD-SiN$_x$ layer cannot be operated, because a-IGZO films become too conductive for channel by diffusion of hydrogen from the PECVD-SiN$_x$ layer during annealing process [11], similar to a-IGZO films with PECVD-SiN$_x$ deposited directly on it [12]. Since a-IGMO films have carrier density remarkably smaller than that of a-IGZO, the effect of PECVD-SiN$_x$ raises carrier density of a-IGMO to optimum value for TFT operation. Therefore, a-IGMO can be a candidate of TFT channel material endurable against processes in reductive environment.

We attempted to carry out BJTS to obtaining information about bandgap and in-gap-state in the amorphous oxide semiconductors, i.e., a-IGMO and a-IGZO. Unfortunately, conductivity of a-IGMO films was too low to measure tunnel conductance with our BJTS set-up. Only the a-IGZO film sample having the highest conductivity (a-IGZO (40 nm) on SiN$_x$/Si, annealed at 300 °C in N$_2$) in our sample library [11] was able to measure tunnel conductance. Fig. 5 shows the tunnel-conductance *dI/dV* for the highly conductive a-IGZO film which shows temperature independent conductivity (resistivity) like a degenerate semiconductor. This tunnel spectrum shows non-zero conductance at zero bias, which means that the density of states (DOS) exists at the Fermi level (E_F). It is consistent with the degenerate semiconductor or/and the metal-like (metallic) conduction behavior of this sample. It should be emphasized that an obvious pseudo-gap of DOS (approx. 0.3 eV in width) exists in the vicinity of E_F, although band-gap energy of this material should be much larger (>3 eV). Further study is needed to interpret the observed DOS character of the amorphous oxide semiconductors, a-IGZO and a-IGMO.

IV. SUMMARY
We investigated a-IGMO as a reductive-process-endurable amorphous oxide semiconductor. Films of a-IGMO were prepared by rf magnetron sputtering deposition followed by the reductive post-annealing process using PECVD-SiN$_x$ underlayer. Optical band-gap energies of a-IGMO111 and a-IGMO221 films were larger than that of a-IGZO. Carrier density and Hall mobility of a-IGMO221 films through reductive post-annealing were almost the same degree as those of a-IGZO films. Although the reductive annealing with PECVD-SiN$_x$ layer made a-IGZO a degenerate semiconductor unsuitable for the TFT operation, a-IGMO TFTs successfully operated after this reductive process. The estimated field effect mobilities of the a-IGMO TFTs were 0.42 cm^{2}V^{-1}s^{-1} for a-IGMO111 and of 2.6 cm^{2}V^{-1}s^{-1} for a-IGMO221, which are somewhat smaller than that of the a-IGZO TFTs, but a-IGMO has an advantage of applicability in reductive processes. Tunnel spectroscopy (BJTS) indicated an unprecedented DOS character of a-IGZO. Further studies on DOS characters of oxide semiconductors such as a-IGZO and a-IGMO are needed to understand the electric transport mechanism of them.

REFERENCES
[1] K. Nomura, H. Ohta, A. Takagi, T. Kamiya, M. Hirano, and H. Hosono, "Room-temperature fabrication of transparent flexible thin-film transistors using amorphous oxide semiconductors," *Nature (London)*, vol. 432, pp. 488–492, 2004.

[2] H. Yabuta et al., "High-mobility thin-film transistor with amorphous InGaZnO$_4$ channel fabricated by room temperature rf-magnetron sputtering," *Appl. Phys. Lett.*, vol. 89, 2006, Art. no. 112123.

[3] H. Kumomi, "Transparent amorphous oxide semiconductors," in *Amorphous Oxide Semiconductors*, H. Hosono and H. Kumomi, Eds. Hoboken, NJ, USA: Wiley, 2022, pp. 21–30.

[4] N. Saito and K. Ikeda, "Amorphous oxide semiconductor TFTs for BEOL transistor applications," in *Amorphous Oxide Semiconductors*, H. Hosono and H. Kumomi, Eds. Hoboken, NJ, USA: Wiley, 2022, pp. 457–472.

[5] N. Kimizuka and T. Mohri, "Spinel, YbFe$_2$O$_4$, and Yb$_2$Fe$_3$O$_7$ types of structures for compounds in the In$_2$O$_3$ and Sc$_2$O$_3$–A$_2$O$_3$–BO systems [A: Fe, Ga, or Al; B: Mg, Mn, Fe, Ni, Cu, or Zn] at temperatures over 1000 °C," *J. Solid State Chem.*, vol. 34, pp. 382–384, 1985.

[6] M. Orita, M. Takeuchi, H. Sakai, and H. Tanji, "New transparent conductive oxides with YbFe$_2$O$_4$ structure," *Jpn. J. Appl. Phys.*, vol. 34, pp. L1550–L1552, 1995.

[7] J. E. Medvedeva, "Averaging of the electron effective mass in multicomponent transparent conducting oxides," *EPL*, vol. 78, 2007, Art. no. 57004.

[8] T. Ekino, T. Takabatake, H. Tanaka, and H. Fujii, "Tunneling evidence for the quasiparticle gap in Kondo semiconductors CeNiSn and CeRhSb," *Phys. Rev. Lett.*, vol. 75, pp. 4262–4265, 1995.

[9] J. Kawabata, T. Ekino, Y. Yamada, Y. Sakai, Y. Muro, and T. Takabatake, "Hybridization gaps and antiferromagnetic gap in the Kondo semiconductors CeT$_2$Al$_{10}$ (T = Fe and Os) observed by break-junction tunneling spectroscopy," *Phys. Rev. B*, vol. 92, 2015, Art. no. 201113(R).

[10] J. Tauc, "Optical properties of amorphous semiconductors," in *Amorphous and Liquid Semiconductors*, J. Tauc, Ed. New York, NY, USA: Plenum, 1974, pp. 159–220.

[11] H. Yabuta et al., "Microscopic structure and electrical transport property of sputter-deposited amorphous indium-gallium-zinc oxide semiconductor films," *J. Phys.: Conf. Ser.*, vol. 518, 2014, Art. no. 012001.

[12] A. Sato et al., "Amorphous In–Ga–Zn–O coplanar homojunction thin-film transistor," *Appl. Phys. Lett.*, vol. 94, 2009, Art. no. 133502.